Science Advances

AAAS

advances.sciencemag.org/cgi/content/full/4/3/eaaq0919/DC1

Supplementary Materials for

Hydrophilic directional slippery rough surfaces for water harvesting

Xianming Dai, Nan Sun, Steven O. Nielsen, Birgitt Boschitsch Stogin, Jing Wang, Shikuan Yang, Tak-Sing Wong

Published 30 March 2018, *Sci. Adv.* **4**, eaaq0919 (2018)
DOI: 10.1126/sciadv.aaq0919

The PDF file includes:

Other Supplementary Material for this manuscript includes the following:
(available at advances.sciencemag.org/cgi/content/full/4/3/eaaq0919/DC1)

movies S1 (.mov format).
movies S2 (.mov format).
movies S3 (.mov format).
movies S4 (.mov format).

movies S5 (.mov format).
movies S6 (.mov format).
movies S7 (.mov format).
movies S8 (.mov format).
movies S9 (.mov format).
movies S10 (.mov format).

section S1. Descriptions of movies S1 to S10

Movie S1 shows a number of highly mobile water droplets on tilted hydrophobic and hydrophilic smooth slippery surfaces (tilt angle = 5^o).

Movie S2 shows a comparison of dropwise condensation performance of hydrophobic (left) and hydrophilic smooth slippery surfaces (right), including droplet nucleation, growth, coalescence, and mobility. This movie highlights the importance of hydrophilic surface chemistry in dropwise condensation.

Movie S3 shows a comparison of dropwise condensation performance of nanotextured SHS (left) and hydrophilic smooth slippery surfaces (right), including droplet nucleation, growth, coalescence and mobility. This movie highlights the importance of the slippery interface to dropwise condensation.

Movie S4 shows a comparison of dropwise condensation performance of hierarchical nanotextured SHS (left) and hydrophilic parallel slippery rough surfaces (right), including droplet nucleation, growth, coalescence, and removal. This movie highlights the importance of the lubricant layer infused in the nanotextures of hierarchically structured surfaces in dropwise condensation.

Movie S5 shows a comparison of dropwise condensation performance of hydrophilic smooth slippery surfaces (left) and hydrophilic parallel slippery rough surfaces (right), including droplet nucleation, growth, coalescence, and removal. This movie highlights the importance of high surface area in dropwise condensation.

Movie S6 shows a comparison of fog harvesting performance between hydrophobic (left) and hydrophilic smooth slippery surfaces (right). This movie highlights the importance of hydrophilic surface chemistry on fog harvesting.

Movie S7 shows a comparison of fog harvesting performance of hydrophobic parallel slippery rough surfaces (left) and hydrophilic parallel slippery rough surfaces (right). This movie highlights the importance of surface chemistry for droplet mobility and removal.

Movie S8 shows a comparison of fog harvesting performance of hierarchical superhydrophobic surfaces (left) and hydrophilic parallel slippery rough surfaces (right). This movie highlights the importance of slippery interface on hierarchical structured surface for droplet mobility and removal.

Movie S9 shows a comparison of fog harvesting performance of nanotextured superhydrophobic surfaces (left) and hydrophilic slippery surfaces (right). This movie highlights the importance of slippery interface in fog harvesting.

Movie S10 shows a comparison of fog harvesting performance of hydrophilic smooth slippery surfaces (left) and hydrophilic parallel slippery rough surfaces (right). This movie highlights the importance of high surface area on fog harvesting.

section S2. Design principle of surface structures

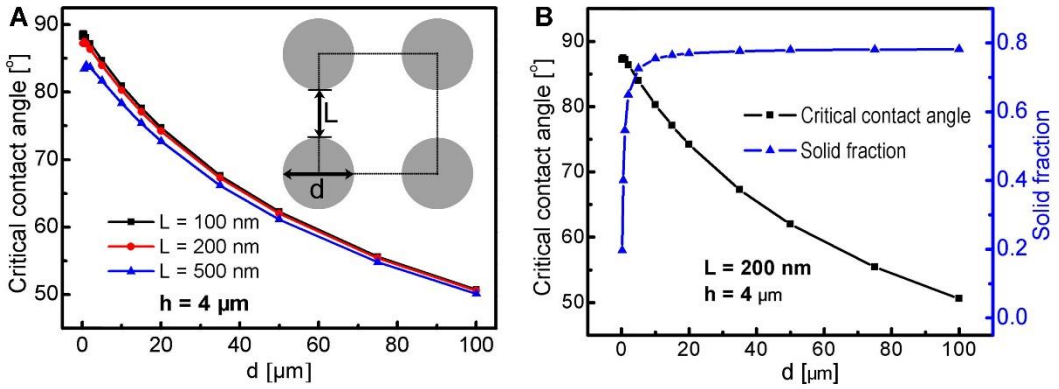

fig. S1. Design principle of the surface structures. (A) Dependence of the critical CA on the average diameter *d* of each pillar. (B) Nanotextures can yield both high critical CA and low solid fraction when *h* ~ 4 μm and *L* = 200 nm.

Consider a silicon surface comprised of an array of round pillars (fig. S1A) with diameter *d*, inter-pillar spacing *L*, and height *h*. The solid fraction φ of the surface can be expressed as $\varphi = \frac{\pi d^2}{4(d+L)^2}$, and the roughness *r* of the surface can be expressed as $r = 1 + \frac{\pi dh}{(d+L)^2}$. To ensure the liquid lubricant is fully infused into the surface textures, the surface structure should be designed to yield a high critical contact angle (CA), θ_c, to enable the complete wetting of liquid lubricant (*i.e.*, $\theta < \theta_c$, where θ is the contact angle of the lubricant on the smooth counterpart of the textured surface). Here the critical CA can be expressed as $\cos\theta_c = \frac{1-\varphi}{r-\varphi}$. Based on this relationship, one can show that both *d* and *L* have to be much smaller than *h* in order to obtain a high critical CA (*i.e.*, $\theta_c \to 90^o$). The typical height of the surface textures is on the order of ~4 μm in our study. Therefore, a high critical CA and small solid fraction will require both the pillar size *d* and inter-pillar spacing *L* to be in the nanometer scale (fig. S1A and B). For example, when *d* = 100 nm, *L* = 200 nm, and *h* = 4 μm, the critical CA is 86.5° and the solid fraction is 0.09 (fig. S1B).

Nanostructures were obtained using a black silicon method (*37)* (fig. S2A). The resulting surfaces were then silanized with perfluorinated silanes in the gas phase to create a surface compatible with the

lubricant we used. We then infused the Krytox perfluorinated lubricant into the nanotextures and removed the excess lubricant at a spin speed of 12000 rpm. The surface became homogeneous and flat (fig. S2B).

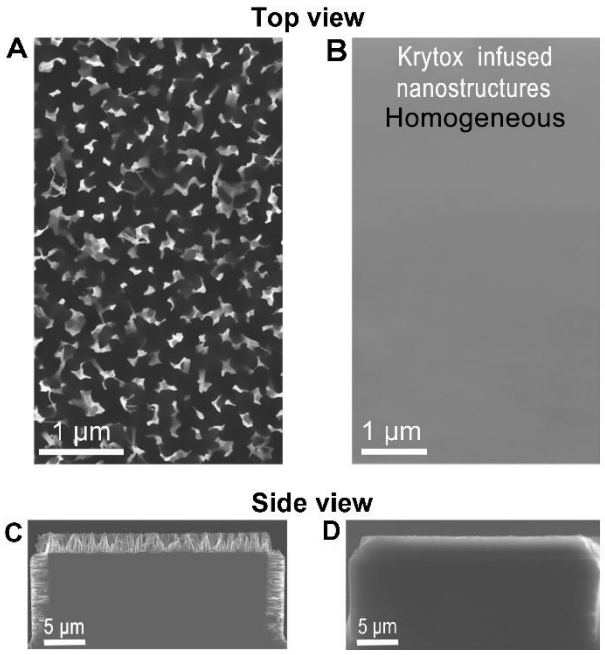

fig. S2. SEM images of nanotextures and SLIPS. (A) Top view of the silicon nanotextures. (B) Top view of the Krytox oil infused nanotextured surface after removing excess lubricant at a spin speed of 12000 rpm. (C) Nanotextures on a micropillar. (D) Liquid-infused nanotextures on a micropillar

Following our discussion, the lubricant on microstructures (without nanostructures on each micropillar) can be easily dewetted, rendering the surface sticky (fig. S3A). In addition, we studied the effect of lubricant thickness on CA measurement. Since the thickness of a given lubricant on the substrate is a function of the spin speed, we control the lubricant thickness by changing the spin speed accordingly. When the lubricant is too thick (spin speed < 1000 rpm), the lubricant interface is deformed, yielding a lower CA than the one predicted by the modified Young equation (fig. S3B). At higher spin speed (> 5000 rpm), excess lubricant was removed from the substrate. The contact angles of water droplets on these lubricated surfaces approach to constant values for increasing spin speed (fig. S3D and main text), and are consistent with the theoretical predictions. Based on this observation, a nanotextured surface with liquid lubrication at a spin speed of > 5000 rpm was used in order to provide a precise wetting characterization. Furthermore, we investigated the effect of a wrapping layer on CA measurement. The

wrapping layer is formed because the low surface tension lubricant preferably cover the high surface tension water droplet. The wrapping layer significantly reduces the CA when the droplet size is comparable to the thickness of the lubricant layer (fig. S3C and main text).

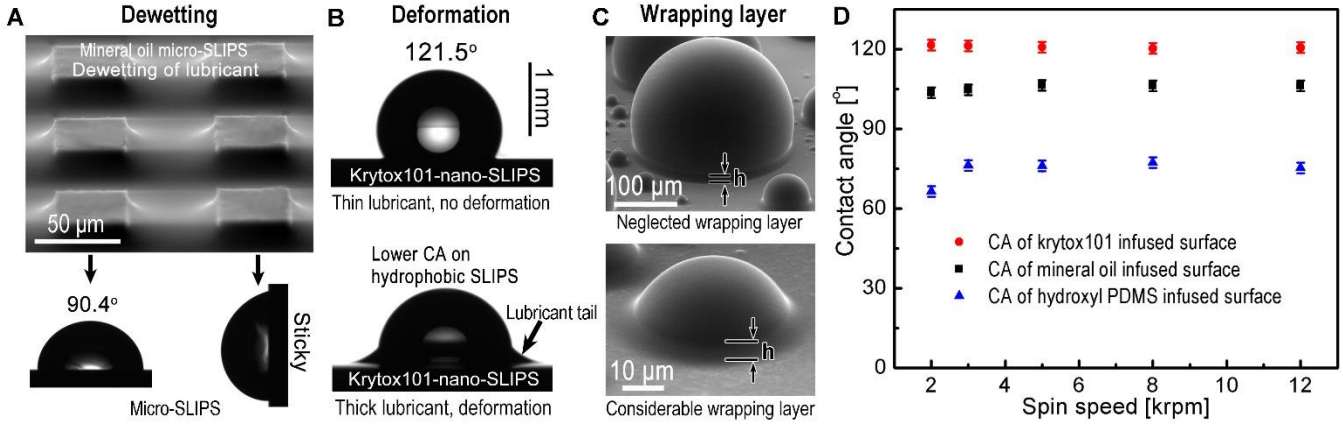

fig. S3. Wetting characteristics on liquid-infused slippery surfaces. (A) Dewetting on a liquid-infused microstructured surface (i.e., micro-SLIPS; length = 52 μm, width = 48 μm, height = 19 μm). The contact angle (θ = 90.4°) on a dewetted mineral oil infused surface was much smaller than the theoretical prediction based on the modified Young's equation (θ = 107.2°). The water droplet was sticky on the dewetted mineral oil infused surface. (B) Deformation effect on the wetting of water droplet on Krytox oil infused nanotextured surface (*i.e.*, nano-SLIPS). When the lubricant is thin (compared to the size of the droplet), the experimental CA can be precisely predicted by the modified Young's equation. When the lubricant is thick (compared to the size of the droplet), the experimental measurements deviate from the theoretical predictions. (C) Environmental electron micrograph of water droplet on Krytox oil infused nanotextured surface. When the droplet is large (compared to the thickness of the lubricant), the wrapping layer effect on the CA is negligible. However, when the droplet is small (compared to the thickness of the lubricant), the wrapping layer is prominent and significantly reduces the CA. Lubricant thickness is denoted as *h*. (D) Influence of lubricant thickness on the water contact angle on liquid-infused nanotextured surfaces. The measured contact angles for a 5 μL water droplet become constant when the spin speed is > 5000 rpm.

section S3. Wetting equations on liquid-infused surfaces

Wrapping layer formation (also called cloaking) may exist on the water droplet depending on whether it is more energetically favorable to have a lubricant layer covering the water droplet. Even though some work showed the existence of wrapping layer at the microscale (*26)*, we found that the wrapping layer (if one exists) did not affect our macroscopic contact angle predictions based on the modified Young's equation. One possible reason is that for large water droplets (> 5 μL, water; droplet diameter > 1 mm),

the wrapping layer (if one exists) does not cover a large percentage of the surface. Therefore, its presence does not significantly affect the macroscopic contact angle predictions, which are strongly supported by our experimental measurements.

To further illustrate our point, we present two different models to predict the apparent contact angles: one is when the wrapping layer is absent (fig. S4A, B) and the other is when a thin wrapping layer is present (fig. S4C). Based on these two models, we have computed the corresponding apparent contact angles and compared them with the experimental values as shown in table S1. Note that for most of the lubricants we used, the interfacial tensions at the water-gas interface are very similar to the sum of the interfacial tensions at oil-gas and oil-water interfaces (i.e., $\gamma_{WG} \approx \gamma_{OG} + \gamma_{OW}$). Therefore, both proposed relations can predict most of the experimental contact angles (table S1). However, for lubricants that do not form a wrapping layer (i.e., ionic liquid (*8*)), it is shown that the model without considering the wrapping layer can achieve a much better prediction.

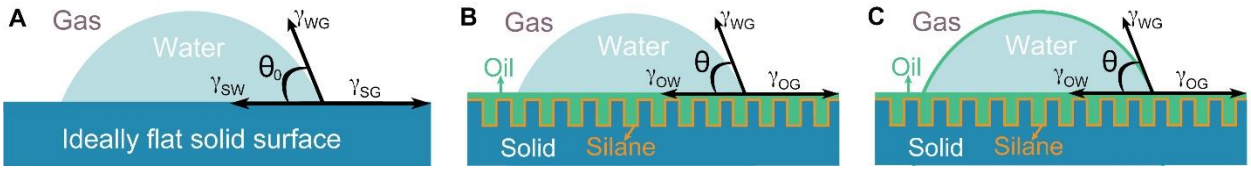

$$cos\theta_0 = \frac{\gamma_{SG}-\gamma_{SW}}{\gamma_{WG}} \qquad cos\theta = \frac{\gamma_{OG}-\gamma_{OW}}{\gamma_{WG}} \qquad cos\theta^* = \frac{\gamma_{OG}-\gamma_{OW}}{\gamma_{OG}+\gamma_{OW}}$$

fig. S4. Wetting models of a water droplet on difference surfaces. (A) Ideally flat solid surface. (B) Liquid-infused nanotextured surface without a wrapping layer. (C) Liquid-infused nanotextured surface with a thin wrapping layer.

table S1. CAs and thermal conductivities of different lubricants used in this study.

Lubricant	Thermal conductivity [W/(m·K)]	Experimental contact angle [°]	$cos\theta = \frac{\gamma_{OG} - \gamma_{OW}}{\gamma_{WG}}$	$cos\theta^* = \frac{\gamma_{OG} - \gamma_{OW}}{\gamma_{OG} + \gamma_{OW}}$
Krytox 101	~0.08 – ~0.09 [1]	121.5 ± 1.2	123.1 ± 2.2	122.5 ± 2.2
Hydride PDMS	-	110.6 ± 1.1	109.0 ± 2.2	111.6 ± 2.2
Mineral oil	-	106.3 ± 0.5	107.3 ± 1.2	105.8 ± 1.3
Hexadecane	-	105.9 ± 0.8	106.3 ± 1.2	105.9 ± 1.2
Silicone oil	-	104 ± 0.8	104.0 ± 1.8	106.6 ± 1.8
Hydroxy PDMS-95	-	98.6 ± 0.6	96.9 ± 2.2	99.6 ± 2.2
Hydroxy PDMS-65	-	95.8 ± 0.5	94.2 ± 2.2	96.2 ± 2.2
Hydroxy PDMS-25	~0.15 [2]	76.2 ± 0.9	78.7 ± 2.4	59.7 ± 2.4
Ionic liquid	-	57.2 ± 1.2	58.2 ± 2.0	49.4 ± 2.0

Note: [1] Krytox Performance Lubricant Specification Sheet. Available online at https://www.chemours.com/Lubricants/en_US/assets/downloads/H-58505-4_Krytox_Overview_LowRes.pdf;

[2] C. Roberts, A. Graham, M. Nemer, L. Phinney, R. Garcia, E. Stirrup, Physical Properties of Low-Molecular Weight Polydimethylsiloxane Fluids, Sandia Report (SAND 2017-1242) (2017), available online at http://prod.sandia.gov/techlib/access-control.cgi/2017/171242.pdf

[3] At least three independent measurements were conducted for the contact angle measurements.

section S4. Design of SRS

We have designed three different SRS: lubricated micropillar arrays (isotropic SRS), lubricated microgrooves perpendicular to the droplet sliding direction (perpendicular SRS), and lubricated microgrooves parallel to the sliding direction (parallel SRS) (fig. S5A, B). The contact angle hysteresis on parallel SRS is as low as that on SLIPS. However, the surface area of parallel SRS is much larger than that of SLIPS. Therefore, we utilized parallel SRS for the condensation and fog harvesting studies. The hierarchical structures of the SRS were fabricated on a p-type <100> silicon wafer using deep reactive-ion etching (DRIE) and wet etching (*25)*, while the nanostructures of SLIPS were fabricated using the black silicon method (*37)*. We used hydroxy PDMS with the viscosity of 25 cSt for all the slippery rough surfaces and SLIPS.

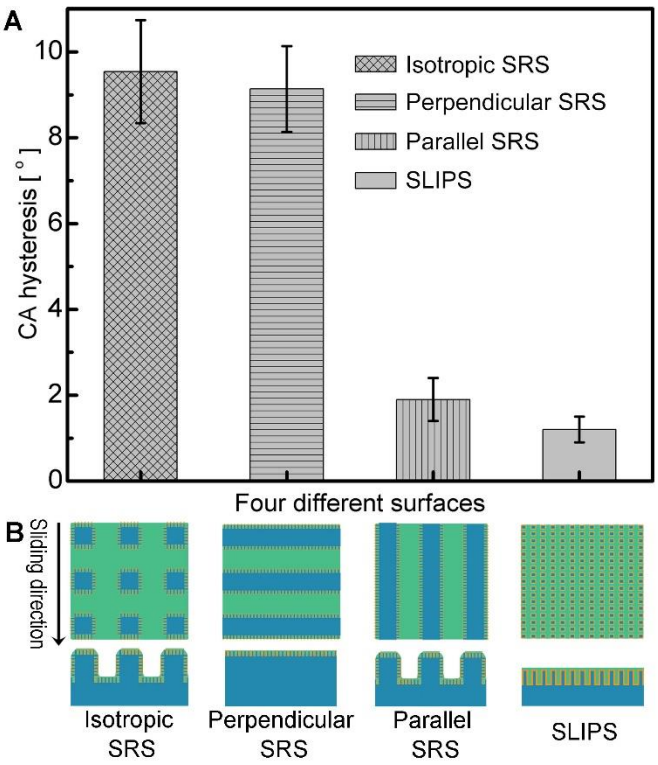

fig. S5. Design of directional SRS. (A) CA hysteresis of water droplets on various hydroxy PDMS lubricated surfaces. Advancing and receding angles were evaluated by viewing the droplet from an angle perpendicular to the sliding direction. (B) Top view and side view of four different slippery surfaces, including liquid-infused micropillars (isotropic SRS), perpendicular microgrooves (perpendicular SRS), parallel microgrooves (parallel SRS), and nanotextures (SLIPS).

section S5. Longevity of SRS

There are two ways to further enhance the longevity of the lubricant-infused slippery rough surfaces (SRS) – one is by engineering the surface textures for lubricant retention and the other is by tuning the lubricant viscosity. To experimentally verify these factors, we have investigated the longevity of the lubricant-infused in the SRS through continuous droplet shedding. Specifically, if the lubricant is carried away significantly by the shedding droplets over time, then the liquid repellency of the surfaces will be degraded (as reflected by an increase in the sliding angle of the droplets). As illustrated in fig. S6A, it was observed that the lubricant longevity can be significantly improved by the presence of nanotextures owing to the enhanced capillary force for lubricant retention. The SRS can maintain the liquid repellency even after continuous shedding of 1000 droplets. In comparison, the lubricant was taken away gradually by the shedding of foreign contacting droplets for surfaces without nanostructures.

We also demonstrated that the lubricant longevity can be further improved by using a more viscous lubricant. For example, we have measured the evaporation rates for three types of hydroxy polydimethylsiloxane (PDMS) with increasing viscosities (i.e., from 25 cSt to 95 cSt) using a high-resolution analytical balance (Mettler Toledo XP504 DeltaRange, resolution = 0.1 mg). We have conducted experiments to monitor the evaporation of the lubricants under static, ambient conditions. We define the relative mass of lubricant, M^*, as the residual lubricant weight in the textures at an instant in time $M(t)$ normalized by the original lubricant weight M_0, i.e., $M^*(t) = M(t)/M_0$, where t is time. While the relative mass of hydroxy PDMS (25 cSt) is reduced by ~20% over the course of 14 days, our measurements showed that we could substitute the hydroxy PDMS (25 cSt) with the ones with higher viscosities (viscosity 65 cSt or 95 cSt) to minimize the effect of lubricant evaporation (fig. S6B).

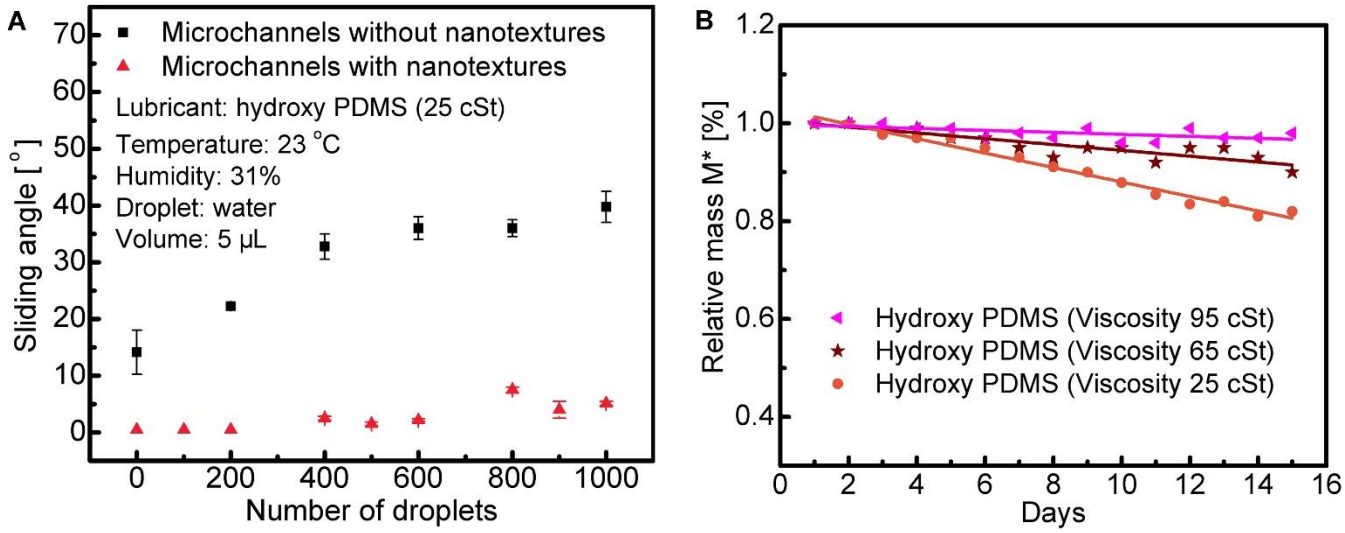

fig. S6. The effect of nanotextures on lubricant retention. (A) Effect of nanotextures on lubricant retention. (B) Mass loss of various hydroxy PDMS lubricants due to evaporation in air for 14 days.

section S6. MD simulations for droplet nucleation

We have conducted theoretical analysis and molecular dynamics (MD) simulations to strengthen the nucleation mechanisms on our liquid-infused surfaces. Specifically, our MD simulations demonstrate that the interactions between water molecules and hydrophilic surface functional groups are the key for the nucleation mechanism on the liquid-infused surfaces.

Existing knowledge of dropwise condensation has shown that contact angle is an important factor for nucleation, i.e., a hydrophilic surface (with contact angle of a water droplet less than 90^o) is favorable for nucleation (*2)*. To study the nucleation mechanism with MD simulations, we modeled four different surface chemistries using the terminal group on a self-assembled monolayer (SAM). Namely, we characterize the influence of different functional groups on nucleation by using a well-defined surface, in analogy to the recent work of Zhu et al. (*40)*. In our simulation, the SAM surface is kept at 373 K while the initial water vapor temperature is set at 450 K.

The hydrophobic surfaces (for example, the $–CF_3$ terminated SAM) display a complex behavior which involves predominately homogeneous nucleation – specifically kinetic energy is removed from water (vapor) molecules when impacting onto the cool surface, but the attraction force of the water molecules to the surface is weak so that these molecules typically return to the vapor phase and provide nucleation sites for the formation of clusters within the vapor phase (fig. S7A). Only when a large enough cluster of around 50 ± 20 water molecules encounters the surface does it finally attach onto the surface, and at that point the cluster continues to grow while maintaining a high contact angle (fig. S7B).

On a hydrophilic surface (–OH terminated SAM), the nucleation mechanism is completely different (fig. S7C). The surface and water interactions are now significant, and small clusters formed on the surface do not return to the bulk vapor phase; therefore, the formation of clusters within the bulk vapor phase is suppressed. This greatly speeds up the water condensation process (on the surface) because essentially no homogeneous nucleation occurs in the vapor phase. Also, the contact angle of the droplets formed on the surface are consistent to that of a hydrophilic surface, i.e., the water spreads on the surface instead of beading up. This also enhances the vapor condensation rate because on hydrophobic surfaces the water vapor tends to condense on the existing droplet(s) which are prevented from spreading due to the surface hydrophobicity, whereas on hydrophilic surfaces the existing droplets have a larger surface area and the water vapor can also condense on bare surface regions (fig. S7D).

Based on the composition of the hydroxy PDMS we used in our experiments, we constructed a SAM surface that consists of randomly distributed 80% $–CH_3$ and 20% –OH functional groups to model the functional group distribution of hydroxy PDMS. Three different randomly generated surfaces were constructed, each using a different seed for the random number generator so that the –OH functional sites were in different locations. This lets us conduct three separate simulations to ensure that our results were not overly biased by any one choice of the functional group assignments. Water condensation occurs in the vicinity of the –OH sites as seen in fig. S7E. These sites enhance the condensation rate significantly, as seen in table S2. Overall, our MD simulations provide strong support that the hydrophilic slippery surfaces can perform much better in droplet nucleation because the hydroxy PDMS contains around 20% –OH functional groups, which can significantly enhance the nucleation rate (fig. S7F).

Furthermore, we conducted quantitative analysis from the MD simulations on the nucleation rates on surfaces with different functional groups. Specifically, the time it takes for most (70%) of the water vapor to condense on the surface is reported in table S2 as an average of 9 simulations for each functional group (except for the hydroxy PDMS surface where only 3 simulations were conducted). Our data shows a trend that the more hydrophilic the surface is, the faster the vapor condenses. However, the vapor condensation rate varies non-linearly with respect to the contact angles of the respective surfaces (table S2).

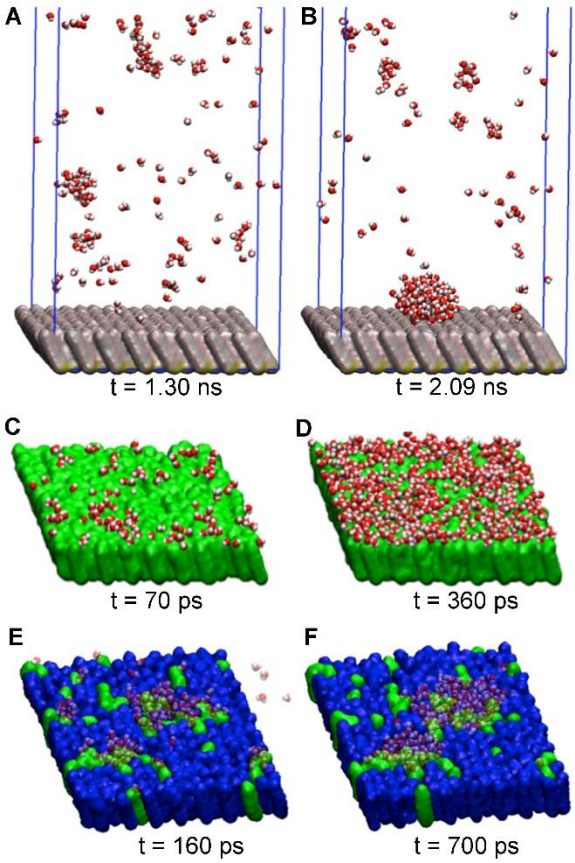

fig. S7. Nucleation on various functionalized surfaces. (A) Nucleation on the surface consisting of –CF_3 functional groups (macroscopic contact angle 118^o). Small water clusters are seen in the bulk vapor phase reminiscent of homogeneous nucleation, although the surface is crucial in removing kinetic energy from water molecules to allow these clusters to form. (B) A droplet is captured by the surface and grows larger while maintaining a contact angle consistent to that of a hydrophobic surface (albeit with large fluctuations due to its small size). (C) Water condenses at 70 ps and (D) spreads uniformly at 360 ps on the surface consisting of –OH functional groups. Nucleation on the surface consisting of 80% –CH_3 (dark blue) and 20% –OH (green) functional groups. Water is observed to nucleate directly in the vicinity of the –OH groups at (E) 160 ps and (F) 700 ps. Note that the water molecules are shown transparent so that the underlying surface functional groups are not obscured.

table S2. Time for most (70%) of the water vapor molecules to condense on the SAM surfaces.

SAM terminal group	Condensation time (ps)	Macroscopic contact angle (degrees)
–CF_3	2247 ± 469	118
–CH_3	2004 ± 256	112
–OH	129 ± 13	< 15
80% –CH_3, 20% –OH	301 ± 61	< 90